Oceanic plateau model for continental crustal growth in the Archaean: A case study from the Kostomuksha greenstone belt, NW Baltic Shield

Article *in* Earth and Planetary Science Letters · February 1998

DOI: 10.1016/S0012-821X(97)00202-1

CITATIONS
204

READS
427

6 authors, including:

Igor S. Puchtel
University of Maryland, College Park
159 PUBLICATIONS **5,219** CITATIONS
SEE PROFILE

Albrecht W. Hofmann
Max Planck Institute for Chemistry
329 PUBLICATIONS **37,862** CITATIONS
SEE PROFILE

Klaus Mezger
Universität Bern
427 PUBLICATIONS **18,820** CITATIONS
SEE PROFILE

Klaus Peter Jochum
Max Planck Institute for Chemistry
389 PUBLICATIONS **13,625** CITATIONS
SEE PROFILE

ELSEVIER

Earth and Planetary Science Letters 155 (1998) 57–74

EPSL

Oceanic plateau model for continental crustal growth in the Archaean: A case study from the Kostomuksha greenstone belt, NW Baltic Shield

I.S. Puchtel [a,*], A.W. Hofmann [a], K. Mezger [a], K.P. Jochum [a], A.A. Shchipansky [b], A.V. Samsonov [c]

[a] *Max-Planck-Institut für Chemie, Abteilung Geochemie, Postfach 3060, D-55020 Mainz, Germany*
[b] *GIN Russian Academy of Sciences, Pyzhevsky 7, 109017 Moscow, Russian Federation*
[c] *IGEM Russian Academy of Sciences, Staromonetny 35, 109017 Moscow, Russian Federation*

Received 7 April 1997; revised 17 October 1997; accepted 9 November 1997

Abstract

Field studies combined with chemical and isotope data indicate that the Kostomuksha greenstone belt in the NW Baltic Shield consists of two lithotectonic terranes, one mafic igneous and the other sedimentary, separated by a major shear zone. The former contains submarine komatiite–basalt lavas and volcaniclastic lithologies, and the latter is composed of shelf-type rocks and BIF. Komatiitic and basaltic samples yield Sm–Nd and Pb–Pb isochron ages of 2843 ± 39 and 2813 ± 78 Ma, respectively. Their trace-element compositions resemble those of recent Pacific oceanic flood basalts with primitive-mantle normalized Nb/Th of 1.5–2.1 and Nb/La of 1.0–1.5. This is in sharp contrast with island arc and most continental magmas, which are characterized by $Nb/(Th,La)_N \ll 1$. Calculated initial Nd-isotope compositions ($\epsilon Nd(T) = +2.8$ to $+3.4$) plot close to an evolution line previously inferred for major orogens (''MOMO''), which is also consistent with the compositions of recent oceanic plateaux. The high liquidus temperatures of the komatiite magmas (1550°C) and their Al-depleted nature require an unusually hot (1770°C) mantle source for the lavas (> 200°C hotter than the ambient mantle at 2.8 Ga), and are consistent with their formation in a deep mantle plume in equilibrium with residual garnet. This plume had the thermal potential to produce oceanic crust with an average thickness of ~ 30 km underlain by a permanently buoyant refractory lithospheric mantle keel. Nb/U ratios in the komatiites and basalts calculated on the basis of Th–U–Pb relationships range from 35 to 47 and are thus similar to those observed in modern MORB and OIB. This implies that some magma source regions of the Kostomuksha lavas have undergone a degree of continental material extraction comparable with those found in the modern mantle. The mafic terrane is interpreted as a remnant of the upper crustal part of an Archaean oceanic plateau. When the newly formed plateau reached the active continental margin, its upper part collided with the sedimentary terrane but was too buoyant to subduct. As a result, the volcanic section of the plateau was imbricated and obducted thus becoming a new segment of continental crust. The deeper zones were delaminated and tectonically underplated or subducted. © 1998 Elsevier Science B.V.

Keywords: komatiite; mantle plumes; oceanic crust; isotopes; Archean

* Corresponding author.

PII S0012-821X(97)00202-1

1. Introduction

In the context of the modern paradigm of plate tectonics, the formation of new continental crust has generally been thought to occur *continuously* at island arcs, which form during the subduction of oceanic plates into the mantle [1]. Subduction generates crust by extracting melts from the mantle overlying the subducted plate (and possibly from the plate itself). More recently, an alternative mechanism has been proposed, which involves the lateral accretion of oceanic plateaux formed as a result of *periodic* catastrophic outpouring of mafic magmas onto the ocean floor [2–8]. According to this model, the heads of mantle plumes originate deep in the mantle, perhaps at the core–mantle boundary, and produce extremely large amounts of basaltic and komatiitic melts. These erupt very rapidly and create large igneous provinces in the oceans. Oceanic plateaux have diameters often exceeding 1000 km and thicknesses approaching those of normal continental crust. Schubert and Sandwell [9] calculated that the volume of all existing plateaux formed over a 100 Ma period is equivalent to 4.9% of the present continental crust volume, and corresponds to an accretion rate of 3.7 $km^3\ yr^{-1}$. At such rates, a volume equivalent to the entire continental crust could be generated within < 2 Ga by plateau accretion only. Moreover, the Ontong Java rate of emplacement has exceeded the contemporaneous global production rate of the entire mid-ocean ridge system [10]. Because oceanic plateau formation involves more melting than the generation of normal oceanic crust at mid-oceanic ridges, the lithosphere of those plateaux is inferred to be more depleted and thus more buoyant. Therefore, they have the potential to resist subduction and to be accreted laterally to continents by the processes of plate tectonics, thus becoming new fragments of continental crust.

Although several authors have previously suggested that some Archaean greenstone belts might represent accreted fossil oceanic plateaux (see references above), geochemical data relevant for comparisons between Precambrian greenstones and bona fide oceanic plateaux are still quite scarce. One exception is the well-studied Abitibi belt in Canada [11,12], which does show close chemical similarities. In this study we provide new field, isotope and geochemical evidence from another Archaean terrane, which support the involvement of oceanic plateaux in the formation of continental crust.

2. Geological background

The Baltic Shield is subdivided into three main domains, the Caledonian, Svecofennian, and Archaean Domain. The latter includes the Karelian, Belomorian, and the Kola Peninsula provinces [13]. The Karelian province is a typical gneiss–greenstone terrane. It occupies a total area of $\sim 350{,}000\ km^2$ in the SE Baltic Shield (Fig. 1) and is composed of a gneiss–migmatite and a granite–greenstone unit. The latter is made up of volcanic rocks and metasediments of Archaean greenstone belts. These show a pronounced linear alignment forming a pattern of NNW-trending outcrops of isolated relict structures among the granitoid rocks of the gneiss–migmatite unit.

The Gimola–Kostomuksha greenstone belt consists of several conjugate synforms that can be traced from the city of Kostomuksha southwards over a distance of > 400 km; the Kostomuksha synform is the largest of these. It is clearly asymmetric; the thickness of the supracrustal sequence ranges from 3.5 km on the western limb to several hundred meters on the eastern limb. The metamorphic grade increases from greenschist facies in the center to amphibolite facies along the margins. Previous stratigraphic reconstructions implied that the belt contained an undisrupted sequence of the lower volcanic group referred to as the Kontokky series, and the upper sedimentary group of the Gimola series [14]. More recent work [15] has demonstrated a more complex stratigraphic and structural framework of the belt. It consists of at least two distinct lithotectonic terranes, the Kontokky and the Gimola terrane (Fig. 2).

The Kontokky terrane is composed of a steeply dipping homoclinal sequence, which includes mafic–ultramafic lavas and volcaniclastic lithologies and minor felsic lavas and tuffs. Numerous gabbro and peridotite sills form an integral part of the volcanic succession. Contacts between the Kontokky terrane and adjacent TTG-gneisses are entirely tectonic in character.

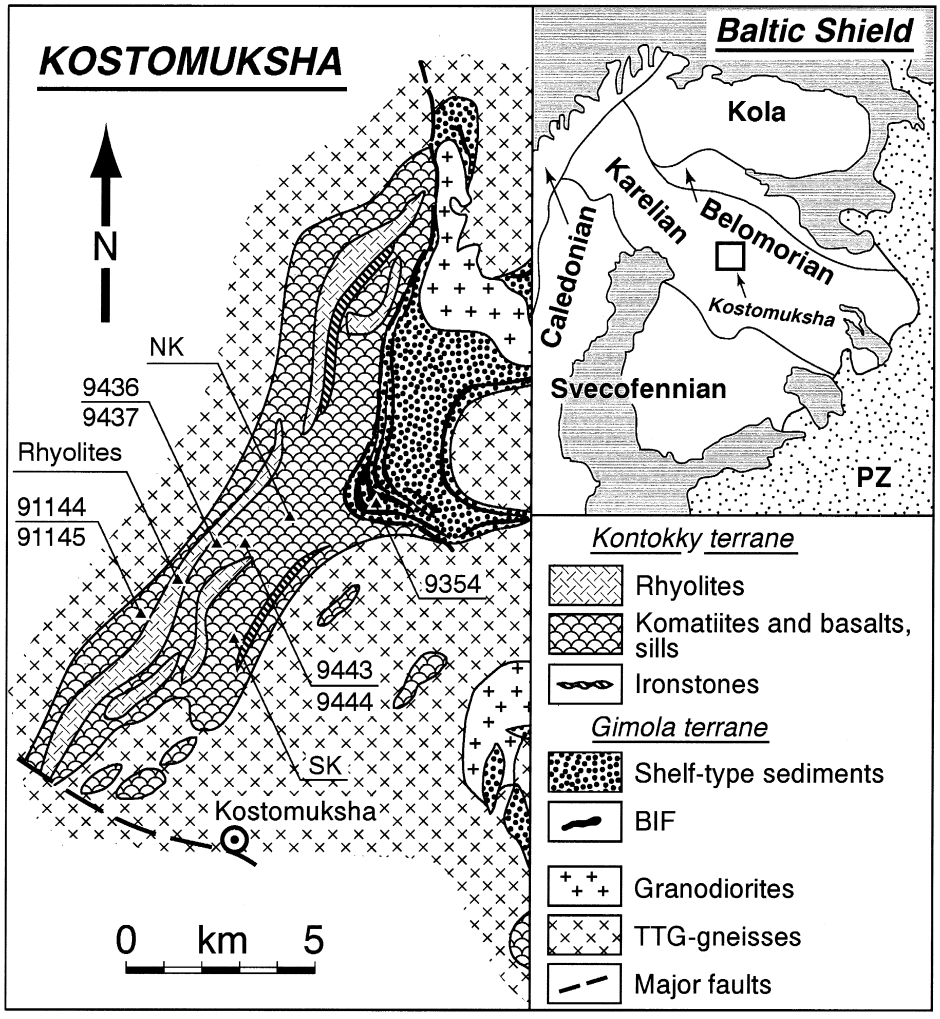

Fig. 1. Geologic–petrographic map of the Kostomuksha synform and the location of sampled outcrops and drillholes. *NK, SK* = Northern and Southern komatiites, respectively.

The mafic volcanic rocks constitute 70% of the sequence and are represented by pillow, variolitic and massive tholeiites. Lava flows with a lower massive portion and a pillowed upper part ranging in thickness between 4 and 10 m are most common. In the variolitic lavas, the varioles are unevenly distributed and range in size from 0.5 to 1–2 cm.

The komatiitic rocks occur as lava horizons several hundred meters thick in the middle and upper parts of the sequence. Primary minerals are replaced pseudomorphically, so that the morphology of original minerals and the textural features of the rocks can be readily identified. Single komatiite lava flows are either massive or differentiated. Massive flows are normally thicker (up to 20 m) and are composed of uniform olivine-porphyritic komatiite. They usually display polyhedral joint blocks decreasing in size from 1 to 0.2 m towards the flowtop. Differentiated flows are rarely more than 6 m thick. Most flows consist of a flowtop breccia, spinifex and cumulate zones. The flowtop is sometimes up to 1 m thick and represents a true volcanic breccia. It originated during interaction of outpouring lava with seawater and contains glassy lava fragments in a

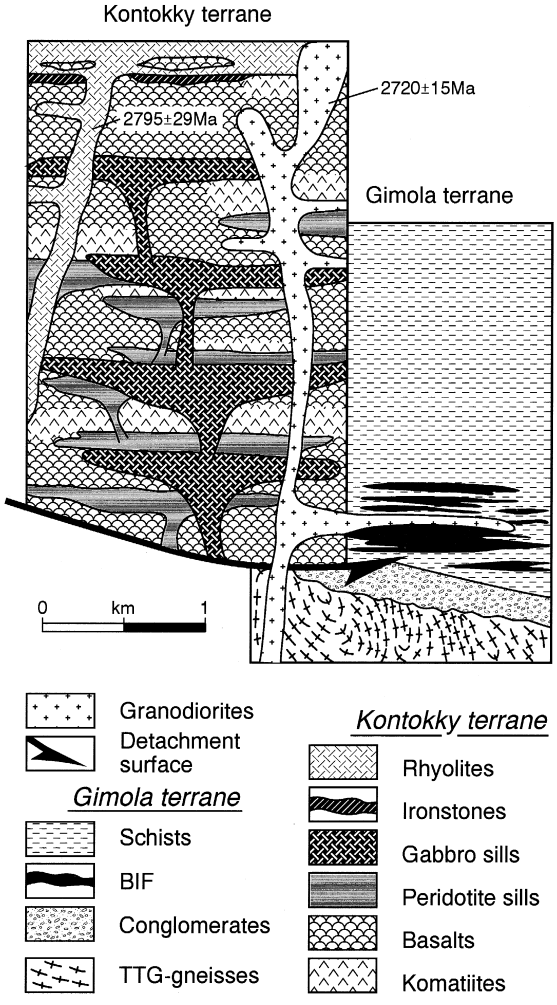

Fig. 2. Generalized stratigraphic section of the Kostomuksha greenstone belt showing the two terranes and the location of proposed detachment surface.

now chlorite-rich matrix. The spinifex zone consists of the upper chilled margin with olivine microspinifex texture, which grades downwards into the random and oriented-plate olivine spinifex layers. The cumulate zone is a massive olivine-porphyritic rock consisting of rather loosely-packed olivine phenocrysts embedded in a glassy groundmass.

A minor component of the volcanic sequence are several thin horizons of ash flow and lapilli komatiite tuffs. They are represented by finely- to coarsely-bedded or breccia-like rocks consisting of subangular glassy fragments in a fine-grained matrix.

Felsic rocks within the Kostomuksha belt are represented by subvolcanic, volcanic and volcaniclastic lithologies of dacite–rhyolite composition. On the basis of field relationships Samsonov et al. [16] have concluded that they intrude and overlie the mafic–ultramafic lavas. The U–Pb age of 2795 ± 29 Ma for zircons from felsic lavas defines the time of their emplacement.

The Gimola terrane consists largely of shelf-type sedimentary rocks. The base is marked by coarse to rhythmically alternating pebbly conglomerates, grits, psammites and carbonaceous phyllite-like shales. These grade upwards into a 2 km thick banded iron formation. The BIF comprises magnetite–pyrrhotite quartzites intercalated with rhythmically bedded sandstone–clay terrigenous flysch sediments and is host to the Kostomuksha iron deposit. Both terranes were intruded by late-tectonic granodiorites with a U–Pb zircon age of 2720 ± 15 Ma [16].

The two terranes are separated by a major tectonic detachment surface consisting of a shear zone several meters thick defined by mylonites developed in rocks from both terranes (Fig. 2). We propose that the two terranes moved and were spatially juxtaposed along this zone and that the Kontokky terrane is thus allochthonous. This interpretation is based on several key observations. First, the lavas are deformed to the same extent as the terrigenous sediments with a tectonic contact between the two. Second, the volcanic sequence does not contain any sedimentary interlayers. This indicates that the eruption site of the lavas was remote from any site of terrigenous sediment deposition. Third, the sedimentary terrane shows a compositional change indicating the change in depositional environment as the oceanic plate approached the continental margin. We interpret this geological situation as representing an ancient accretionary complex similar to that described by Kimura et al. [17] for the Abitibi belt in Canada.

3. Analytical procedures

Major-element abundances were determined by XRF using a VRA-20R spectrometer at the Institute of Geology in Novosibirsk. Cr, V, Co, Ni, Zr, Y, Sc, Nb, Rb, Sr, Th, U, and Pb were determined on an

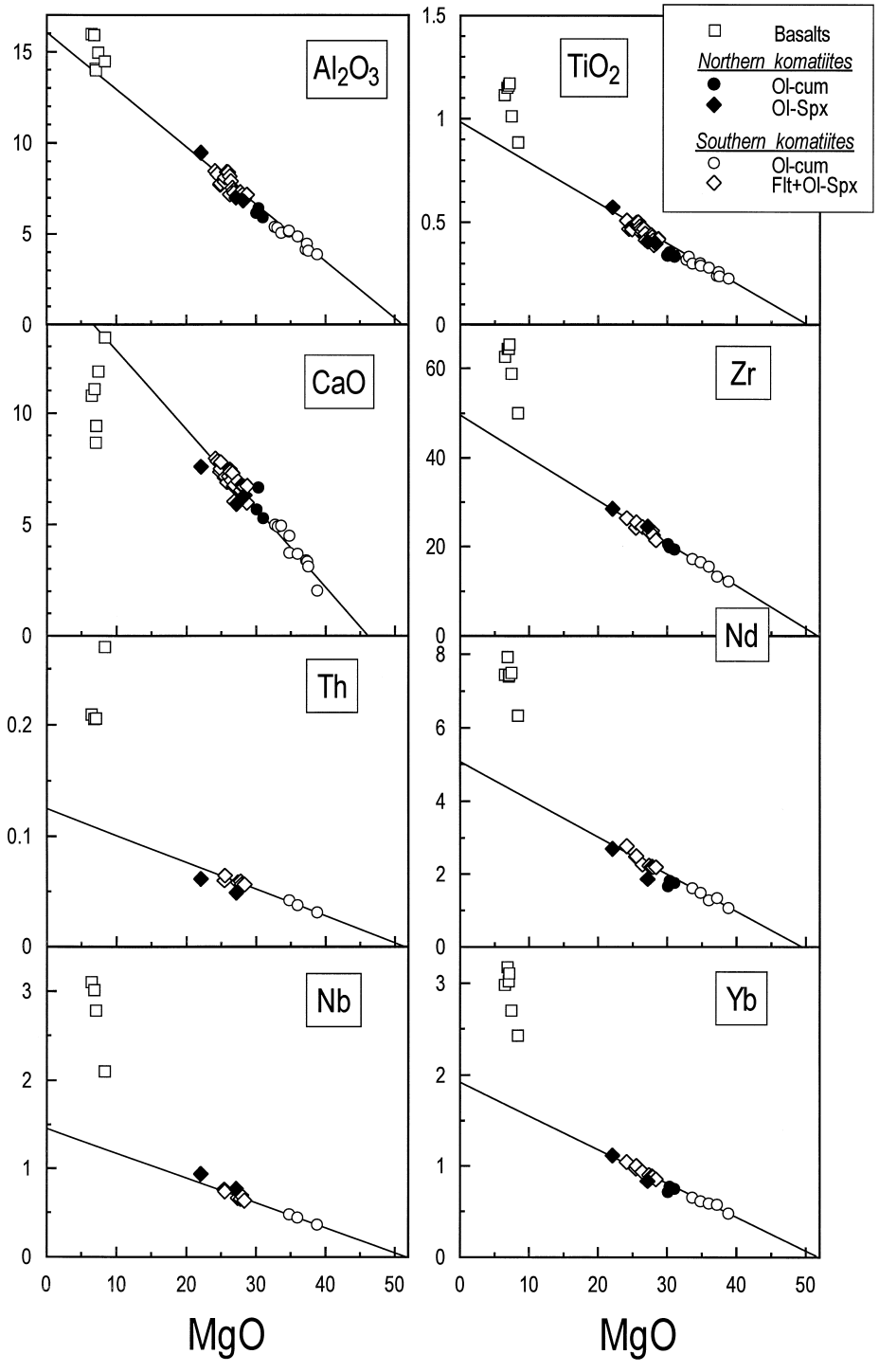

Fig. 3. Variation diagrams for selected major and trace elements.

Table 1
Major- and trace-element data

Sample	Basalts						Northern komatiites					Southern komatiites												
							Ol-porphyritic			Ol-spinifex		Ol-cumulate					Ol-spinifex							
	91144	91145	9436	9437	9443	9444	91154	91157	9332	91155	91156	9454	9457	94100	94118	94126	9479	9493	9496	9498	94104	94111	94114	94123
SiO_2	49.1	47.2	49.8	49.4	50.2	51.1	45.7	45.9	45.4	45.1	45.6	43.5	43.6	43.7	43.6	44.2	44.6	44.7	45.0	44.8	45.3	46.2	45.5	44.7
TiO_2	1.01	0.89	1.11	1.15	1.17	1.16	0.34	0.34	0.35	0.41	0.57	0.28	0.23	0.29	0.24	0.30	0.43	0.46	0.49	0.51	0.41	0.42	0.40	0.50
Al_2O_3	15.0	14.5	16.0	15.9	14.0	14.1	6.18	5.93	6.44	7.01	9.47	4.88	3.89	5.19	4.17	5.07	7.31	7.91	7.89	8.47	7.12	7.15	6.97	8.12
Fe_2O_3	13.6	14.1	13.4	13.3	14.3	14.5	11.9	11.3	10.5	14.1	14.0	11.4	11.2	11.2	11.2	11.6	13.0	13.2	13.8	13.4	12.3	11.7	12.2	13.6
MnO	0.19	0.19	0.20	0.20	0.19	0.19	0.17	0.16	0.17	0.16	0.18	0.18	0.18	0.21	0.19	0.19	0.17	0.17	0.18	0.18	0.18	0.16	0.17	0.17
MgO	7.42	8.37	6.46	6.83	7.10	7.02	30.0	31.0	30.3	27.2	22.1	36.0	38.8	34.8	37.2	33.6	27.8	26.4	25.4	24.1	27.9	27.4	28.3	25.5
CaO	11.9	13.4	10.8	11.1	9.44	8.67	5.67	5.28	6.66	5.93	7.60	3.68	2.03	4.49	3.38	4.94	6.55	6.98	7.12	7.97	6.77	6.95	6.31	7.14
Na_2O	1.48	0.95	1.86	1.80	3.31	2.67	0.01	0.01	0.02	0.02	0.40	0.02	0.02	0.01	0.01	0.01	0.01	0.09	0.01	0.22	0.01	0.04	0.01	0.16
K_2O	0.32	0.35	0.33	0.27	0.30	0.56	0.02	0.02	0.02	0.04	0.06	0.02	0.01	0.02	0.01	0.01	0.02	0.02	0.02	0.03	0.02	0.02	0.02	0.03
P_2O_5	0.08	0.08	0.07	0.07	0.07	0.09	0.05	0.06	0.07	0.06	0.07	0.04	0.03	0.06	0.04	0.05	0.07	0.06	0.07	0.06	0.05	0.08	0.07	0.06
LOI	1.39	2.03	1.06	0.70	0.70	0.73	8.35	7.68	7.60	6.30	5.70	10.98	12.48	10.12	10.85	9.90	7.05	6.27	5.65	5.70	7.69	6.39	7.21	6.11
Cr	**261**	**290**	**261**	**253**	**144**	**143**	**3220**	**2902**	**2859**	**3812**	**3711**	**3276**	**3212**	**2612**	**2430**	**2763**	**3083**	**3120**	**2968**	**3244**	**2946**	**3009**	**2895**	**3250**
V	**314**	**298**	**351**	**358**	**343**	**354**	**153**	**138**	**118**	**202**	**234**	**111**	**88**	**113**	**91**	**125**	**164**	**179**	**171**	**183**	**153**	**183**	**155**	**180**
Co	**53**	**52**	**61**	**61**	**51**	**52**	**103**	**100**	**104**	**113**	**110**	**118**	**132**	**122**	**118**	**115**	**103**	**104**	**99**	**101**	**98**	**101**	**109**	**103**
Ni	**134**	**145**	**129**	**120**	**108**	**106**	**1454**	**1606**	**1609**	**1167**	**1007**	**1892**	**2182**	**1889**	**2145**	**1861**	**1232**	**1244**	**1103**	**1097**	**1378**	**1401**	**1456**	**1175**
Zr	**58.8**	50.0	62.7	64.4	**65.5**	**64.5**	**20.6**	**19.4**	**19.9**	24.5	28.5	15.5	12.2	16.5	**13.3**	**17.2**	**23.6**	**24.4**	24.3	**26.4**	22.6	23.4	**21.4**	**25.5**
Nb		2.10	3.10	3.01	2.78					0.768	0.937	0.443	0.364	0.479			0.654		0.762		0.693	0.665	0.635	0.739
Y	**24.3**	21.6	28.5	29.6	**28.2**	**29.2**	**8.00**	**7.54**	**7.90**	9.57	11.7	**6.00**	4.80	6.61	**5.54**	**6.59**	9.00	**9.56**	10.6	**10.8**	8.60	9.58	**8.40**	**10.4**
Sc		40.4	56.4	48.4						26.3	33.8		16.1	19.0					27.7		26.5	26.3		
Rb	**2.4**	3.4	4.1	1.3	**3.0**	**10.1**	**0.65**	**1.3**	**1.9**	1.3	1.3	**0.50**	0.50	0.41	**2.2**	**2.2**	**2.1**	**2.1**	0.44	**2.1**	0.46	0.72	**2.1**	**1.1**
Sr	**91.3**	87.7	70.7	78.5	**148**	**132**	**24.9**	**14.0**	**19.4**	13.8	16.9	**5.55**	4.50	19.8	**12.2**	**36.3**	**13.9**	**15.9**	19.0	**20.1**	19.4	19.2	**20.4**	**31.8**
Th		0.270	0.209	0.206	0.206					0.0487	0.0613	0.0375	0.0307	0.0417			0.0591		0.0599		0.0564	0.0582	0.0562	0.0643
U		0.0850	0.0594	0.0656	0.0918					0.0190	0.0239	0.0174	0.0167	0.0213			0.0216		0.0213		0.0199	0.0203	0.0197	0.0182
U[a]		0.0896	0.0695	0.0683	0.0684					0.0162	0.0204	0.0125	0.0102	0.0139			0.0196		0.0199		0.0187	0.0193	0.0187	0.0214
Pb		1.76	4.73	4.79						0.285	0.299		0.132	0.238					0.298		0.295	0.281		

La	3.52	2.52	2.97	2.87	2.67	2.62	0.432	0.466	0.488	0.505	0.650	0.412	0.350	0.498	0.477	0.548	0.596	0.635	0.772	0.947	0.676	0.681	0.661	0.734
Ce	9.52	7.30	8.68	8.57	8.13	8.03	1.43	1.58	1.64	1.66	2.33	1.25	1.06	1.57	1.44	1.68	2.04	2.09	2.46	2.94	2.13	2.17	2.16	2.42
Nd	7.50	6.33	7.44	7.92	7.44	7.40	1.67	1.76	1.83	1.87	2.70	1.28	1.06	1.48	1.34	1.62	2.21	2.27	2.48	2.77	2.19	2.24	2.19	2.50
Sm	2.53	2.24	2.65	2.82	2.70	2.67	0.694	0.723	0.759	0.811	1.072	0.519	0.418	0.574	0.513	0.621	0.876	0.913	0.963	1.046	0.858	0.870	0.845	0.970
Eu	0.923	0.756	0.923	0.986	0.950	0.941	0.220	0.239	0.249	0.270	0.353	0.163	0.120	0.193	0.141	0.169	0.216	0.307	0.416	0.440	0.313	0.317	0.312	0.372
Gd	3.48	3.09	3.73	3.95	3.86	3.82	1.00	1.04	1.08	1.21	1.62	0.771	0.615	0.829	0.758	0.905	1.27	1.36	1.40	1.51	1.27	1.29	1.22	1.42
Dy	4.30	3.82	4.63	4.94	4.85	4.73	1.24	1.27	1.33	1.51	1.97	0.966	0.770	1.01	0.928	1.11	1.56	1.66	1.71	1.84	1.57	1.59	1.49	1.74
Er	2.80	2.47	3.03	3.24	3.15	3.08	0.762	0.798	0.833	0.904	1.21	0.614	0.492	0.640	0.596	0.693	0.957	1.02	1.05	1.13	0.956	0.970	0.921	1.08
Yb	2.70	2.43	2.98	3.18	3.11	3.03	0.716	0.750	0.772	0.834	1.12	0.589	0.478	0.614	0.576	0.652	0.889	0.937	0.972	1.04	0.878	0.900	0.853	1.00
$(La/Sm)_N$	0.875	0.709	0.706	0.640	0.622	0.618	0.392	0.406	0.405	0.392	0.382	0.501	0.527	0.546	0.585	0.555	0.429	0.438	0.505	0.570	0.495	0.493	0.493	0.477
$(Gd/Yb)_N$	1.04	1.03	1.01	1.01	1.00	1.02	1.13	1.12	1.13	1.17	1.18	1.06	1.04	1.09	1.06	1.12	1.16	1.17	1.16	1.17	1.17	1.16	1.16	1.15
$(Nb/La)_N$		0.829	1.04	1.04	1.03					1.51	1.43	1.07	1.03	0.957			1.09		0.981		1.02	0.970	0.955	1.00
$(Nb/Th)_N$		1.03	1.95	1.93	1.78					2.08	2.01	1.56	1.56	1.51			1.46		1.68		1.62	1.50	1.49	1.51
Nb/U[a]		23.4	44.6	44.1	40.7					47.5	46.0	35.6	35.7	34.6			33.3		38.3		37.0	34.4	34.0	34.6

Analyses recalculated on an anhydrous basis. Trace elements in bold: measured by XRF; underlined: by MIC–ID–SSMS; others: by ICP–MS; REE: by ID–TIMS. Additional major- and trace-element data can be obtained upon request or as an EPSL Online background data set URL (http://www.elsevier.nl/locate/epsl, mirror site: http://www/elsevier.com/locate/epsl) (see figure captions for the site location).[a]U concentrations calculated from Th/U ratio of 3.01.

upgraded PlasmaQuad PQ1 ICP–MS at the University of Kiel and partly by XRF using a Philips PW-1404 spectrometer at the University of Mainz (Table 1). In several samples, Nb, Th, and U concentrations were measured using the MIC–ID–SSMS technique at the MPI für Chemie in Mainz [18]. REE concentrations were determined at IGEM in Moscow by ID–TIMS. Nd- and Pb-isotope studies were carried out at the MPI für Chemie in Mainz. The details of the analytical procedures applied are published elsewhere [19,20].

4. Results

4.1. Chemical compositions

For chemical and isotope studies, fifty-six samples from the Kontokky terrane were collected from surface outcrops (basalts 91144 and 91145, komatiites 91154–91157 and 9332 from the northern part of the study area referred to as the Northern komatiites, and rhyolites) and from the core of three 300–600 m deep diamond drillholes (basalts 9436–9444 and komatiites 9454–94123 from the southern part of the study area referred to as the Southern komatiites). A representative sample set was obtained for the Southern komatiite sequence with a total thickness of $\sim$ 300 m, where 27 flows were studied. One pebbly conglomerate from the Gimola terrane was also analyzed.

The major- and trace-element data are presented in Table 1 and plotted on Figs. 3 and 4. In the basalts, MgO varies between 6.5% and 8.5%. The MgO content in the Southern komatiites ranges between 26% and 29% in flowtop breccias, between 24% and 29% in olivine spinifex, and between 33% and 39% in olivine cumulates. In the Northern komatiites, the MgO abundances vary between 22% and 28% in the spinifex lavas and between 30% and 31% in the massive flows. Most elements show strong correlations with MgO ($r = 0.95–1.0$) and vary in a manner entirely consistent with fractionation of olivine only. When plotted against MgO, the analytical data for the komatiites fall on the olivine control lines, which intersect the MgO axes at 51.0 $\pm$ 0.9%. The trend for CaO has a somewhat steeper slope. The alkalis, Rb, Sr, Ba, U, and Pb show an essentially irregular behavior.

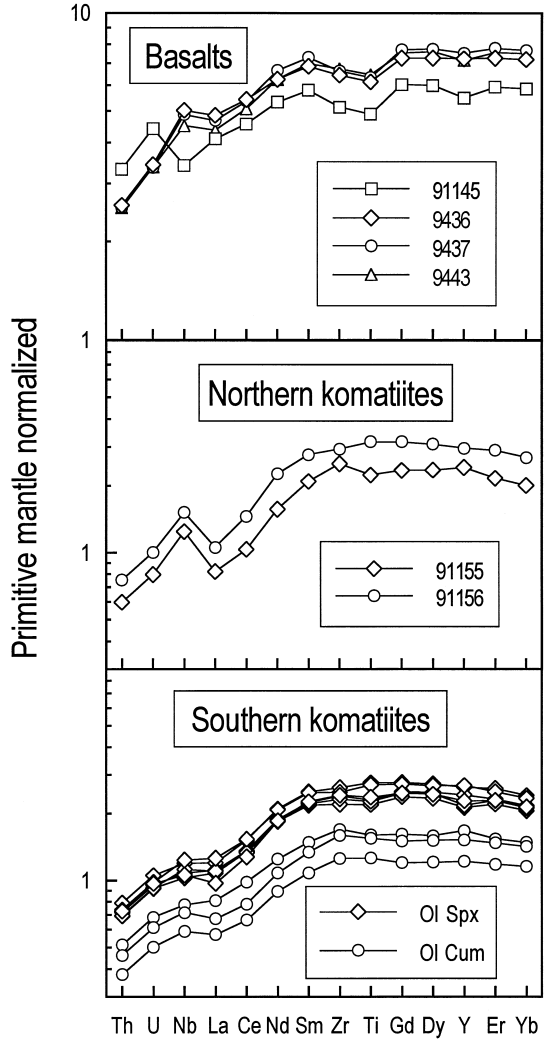

Fig. 4. Concentrations of some major and trace elements normalized to primitive mantle values of Hofmann [63]. U abundances were calculated from Th–U–Pb relationships.

On the whole, the rocks are depleted in the highly incompatible elements LREE, Th and U, and show positive Nb anomalies. Figs. 3 and 4 reveal some differences between the Northern and Southern komatiites and basalts. The most pronounced LREE depletions are recognized in the former; they also exhibit the largest Nb anomalies. The latter are slightly less depleted and reveal smaller Nb anomalies. The basalts are least depleted and, with one exception, are also characterized by pronounced maxima at Nb.

Table 2
Sm–Nd isotope data

Sample	Sm (ppm)	Nd (ppm)	$^{147}Sm/^{144}Nd$	$^{143}Nd/^{144}Nd$	ϵNd(2795)
Northern komatiites:					
91154	0.5271	1.274	0.25003	0.513773±14	2.97
91155	0.7813	1.794	0.26346	0.514021±7	2.97
91156	1.0440	2.601	0.24276	0.513661±5	3.40
91157	0.5605	1.368	0.24769	0.513751±12	3.39
9332	0.5911	1.447	0.24694	0.513721±7	3.07
Southern komatiites:					
9454	0.4563	1.137	0.24277	0.513655±7	3.28
9457	0.4196	1.059	0.23957	0.513572±7	2.81
9479	0.8962	2.251	0.24078	0.513605±6	3.04
9496	0.9979	2.555	0.23612	0.513525±6	3.14
94104	0.7910	2.035	0.23502	0.513499±5	3.03
94111	0.8151	2.101	0.23460	0.513486±5	2.92
94114	0.7845	2.033	0.23335	0.513482±5	3.30
94123	0.9460	2.432	0.23524	0.513503±8	3.03
Basalts:					
91144	2.5380	7.477	0.20522	0.512947±6	2.98
91145	2.2150	6.404	0.20909	0.513014±7	2.90
9436	2.4880	6.961	0.21264	0.513072±5	2.75
9437	2.7940	7.937	0.21283	0.513081±6	2.86
9443	2.7050	7.435	0.21997	0.513211±4	2.82
9444	2.6070	7.251	0.21743	0.513167±5	2.88
Rhyolites:					
134A/93	2.788	15.745	0.10701	0.510870±4	−2.22
136/93	1.547	8.885	0.10522	0.510831±5	−2.35
138/93	2.612	15.325	0.10299	0.510846±6	−1.24
91147	2.151	10.600	0.12271	0.510957±7	−6.21
Pebbly conglomerate:					
9354	3.590	18.97	0.11440	0.511184±3	1.26
Metamorphic minerals:					
91147 Gar	3.341	11.62	0.17381	0.511892±15	
91147 Am	1.942	6.119	0.19183	0.512228±24	
91147 Pl	0.5989	3.092	0.1171	0.510897±9	
91147 Bt	3.801	18.90	0.12157	0.510918±6	

The komatiites have chondritic (= 112) Ti/Zr ratios of 110 ± 6 and show a moderate depletion in Al and Sc (Al/Ti = 17.0 ± 0.6, Ti/Sc = 95 ± 7 compared with 22 and 73 in chondrites). The spinifex-textured and flowtop breccia komatiites are moderately depleted in HREE, while the cumulate samples show less fractionated HREE patterns. The basalts are characterized by flat HREE patterns.

4.2. Isotope data

The Sm–Nd isotope data are presented in Table 2 and plotted in Fig. 5. The komatiites and basalts define an isochron with a slope corresponding to an age of 2843 ± 39 Ma. The samples reveal uniform Nd-isotope compositions with ϵNd(2795) ranging between +2.8 and +3.4. The rhyolites plot below the regression line and are characterized by low

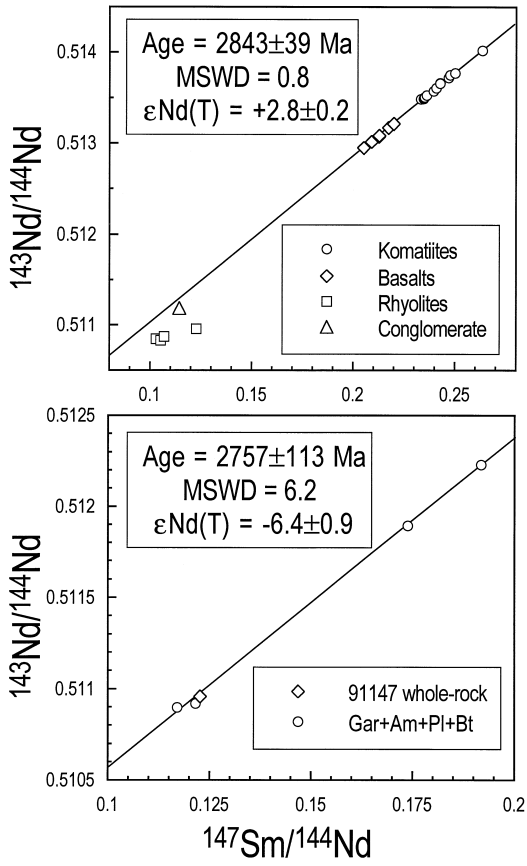

Fig. 5. Sm–Nd isochron diagrams.

ϵNd(2795) of -6.2 to -1.2. This implies that these felsic rocks were derived from LREE-enriched material that records an extended previous residence time in the continental crust. Metamorphic minerals from the rhyolite 91147 define an isochron with an age of 2757 ± 113 Ma corresponding to the time of metamorphic reworking of the sequence. The conglomerate sample has a model T_{DM} age of 3.01 Ga, which corresponds to an average age of the source material of the sedimentary rocks.

Table 3
Pb isotope data

Sample	$^{206}Pb/^{204}Pb$	$^{207}Pb/^{204}Pb$	$^{208}Pb/^{204}Pb$	μ_1
Southern komatiites:				
9479	15.988	15.142	35.321	8.76
9493	15.916	15.134	35.328	8.77
9495	15.716	15.094	35.195	8.77
9496	16.463	15.247	35.738	8.78
9496[a]	16.273	15.202	35.566	8.77
9497	15.986	15.150	35.370	8.78
9498	15.953	15.147	35.390	8.79
94103	15.912	15.124	35.284	8.75
94104	15.948	15.133	35.340	8.75
94109	15.527	15.069	34.937	8.80
94109[a]	15.559	15.067	34.980	8.78
94111	15.781	15.097	35.187	8.75
94111[a]	15.688	15.084	35.098	8.76
94113	15.931	15.158	35.349	8.83
94114	15.792	15.116	35.224	8.79
94114[a]	15.758	15.096	35.122	8.76
94123	15.493	15.046	35.043	8.76
94123[a]	15.436	15.038	34.991	8.77
Basalts:				
9436	14.789	14.912	34.381	8.78
9437	14.911	14.937	34.460	8.78
Leachates:				
9479 3N	15.222	15.016	34.758	8.75
9479 6N	15.225	15.002	34.777	8.71
9495 6N	16.216	15.207	35.621	8.76
9496 1N	17.656	15.466	36.865	8.73
9496 3N	16.766	15.294	35.961	8.72
94109 6N	15.705	15.093	35.257	8.72
94113 1N	17.446	15.418	36.750	8.71
94113 3N	16.386	15.218	35.867	8.71
94123 1N	17.737	15.489	37.097	8.75
94123 3N	16.481	15.235	35.815	8.71

[a]Separate chips from the same sample.

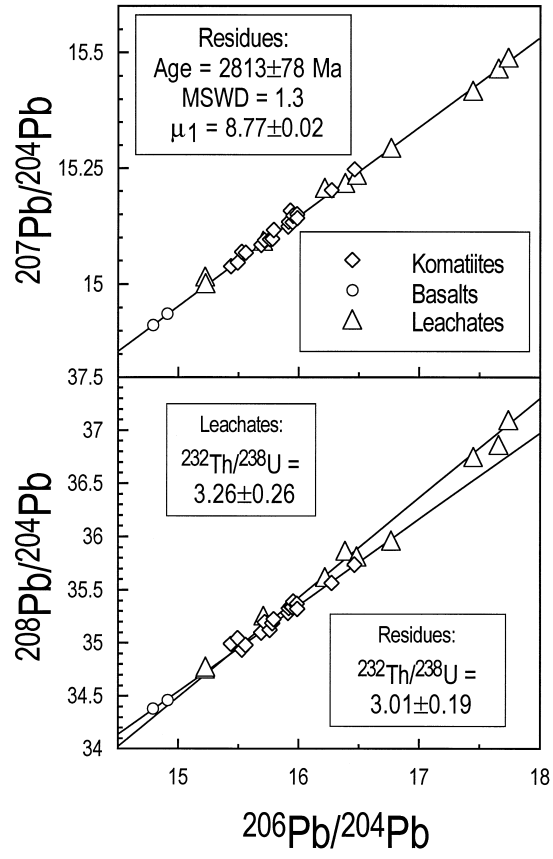

Fig. 6. Pb-isotope data for leachates and residues.

Lead isotopes were measured in leached samples because of the strong possibility of U mobility during low-temperature alteration of submarine lavas. The Pb-isotope data are reported in Table 3 and plotted in Fig. 6. Residues from the komatiites and basalts define an isochron with an age of 2813 ± 78 Ma, in agreement with the U–Pb zircon and Sm–Nd data. Regression of analytical data for the leachates gives a younger age of 2729 ± 62 Ma, which coincides with the Sm–Nd age on metamorphic minerals.

In the $^{208}Pb/^{204}Pb$ vs. $^{206}Pb/^{204}Pb$ plot, the residues and leachates define two regression lines that are barely distinguishable. $^{232}Th/^{238}U$ ratios calculated from the regressions are 3.01 ± 0.19 for the residues and 3.26 ± 0.26 for the leachates. The value for the residues is consistent with the less precise average Th/U ratio of the volcanic rocks (2.6 ± 0.5) calculated from the trace-element data.

5. Discussion

5.1. Eruption environment: subaerial or submarine?

The eruption environment in the Archaean is important because it places constraints on possible tectonic settings. Most documented Archaean lavas are submarine. This suggests that the site of formation of new juvenile crust was in oceanic environment, though some magmas, e.g. at Kambalda and partly at Belingwe, appear to have passed through continental crust.

From field relations it is evident that the Kostomuksha plateau was also submarine. This is obvious from the ubiquitous presence of pillow and variolitic basalts throughout the sequence. Moreover, the presence of thick komatiite flowtop breccias and ash flow tuffs strongly suggests that the komatiite–basalt sequence was accumulated below sea level. Another implication of the ultramafic pyroclastics is very shallow water, probably only a few hundred meters deep.

5.2. Secondary alteration

The Kostomuksha lavas share common features with most Archaean rocks, i.e. they are inevitably modified by secondary alteration processes. Nevertheless, it is possible to monitor their primary chemical compositions. The only liquidus phase in the komatiites is olivine, which controls the composition of the magmas during low-pressure differentiation. Therefore, olivine control lines provide a powerful tool for distinguishing between the igneous and secondary behavior of components (e.g., [21]). When analytical data plot on the olivine control line, this component can be taken as immobile. Thus, it can be shown that the alkalis, Rb, Sr, Ba, U, and Pb were mobile during alteration. A steeper slope of the line in the CaO vs. MgO diagram suggests that CaO was preferentially removed from the samples with higher modal olivine contents as is the case in several other localities (e.g., [12]). All the other elements can be interpreted as immobile.

5.3. Composition of the komatiite liquid and conditions of magma generation

We deduce the composition of the primary komatiite magma using two independent approaches. Flowtop breccias, chilled margins and spinifex layers of komatiite flows are glassy rocks that escaped post-eruption differentiation and therefore have a bulk composition close to that from which the lavas have formed. Calculations of the average composition of these komatiite units from a large number of flows analyzed give $27 \pm 1\%$ MgO. The average composition of equilibrium olivine calculated for individual samples is $Fo_{93.3 \pm 0.7}$.

The second approach is to project the olivine control lines to their intersections with the MgO axis for the elements that are excluded from the olivine crystal lattice. These intercepts directly correspond to the average composition of liquidus olivine. The calculated value is $51.0 \pm 0.9\%$ MgO (average for 14 elements). Recalculating to the olivine stoichiometry, this gives an olivine composition of $Fo_{93.2 \pm 1.0}$. If a $K_{D(ol-liq)}^{Mg-Fe} = 0.31$ [22] is adopted, then olivine with such a composition will be in equilibrium with a liquid containing 26.8% MgO. Thus, two independent lines of evidence suggest that the parental komatiite liquid contained $\sim 27\%$ MgO.

Lower than chondritic Yb/Gd, Al/Ti and Sc/Ti ratios in the Kostomuksha komatiites imply that they belong to the small but important minority of Al-depleted komatiites of late Archaean age that have geochemical affinities resembling those of their early Archaean counterparts. The Al-depleted nature of komatiite melts has been interpreted as a garnet signature since it was first discovered [23]. High pressure stabilizes garnet with respect to pyroxene and olivine [24]. The solubility of garnet in silicate liquids is reduced, and this results in high-pressure magmas that have low concentrations of elements that are compatible with garnet, e.g. Al, HREE, Sc. The relative depletions in these elements can therefore be used to estimate the depths of magma generation. Applying the technique of Herzberg [24] it can be inferred that the komatiite magmas were generated at pressures of ~ 70 kbar, i.e. at a depth of > 200 km. The basalts do not reveal Al depletions and thus were generated at shallower levels. Using the data of McKenzie and Bickle [25] we estimate that the depth of melting initiation of komatiites was 310 ± 50 km, in agreement with the above result. Similar calculations for the basalts give 60 ± 10 km as the initial depth of their melting.

The degree of HREE depletions systematically

decreases in cumulate portions of komatiite flows compared with the spinifex-textured layers (Table 1). The cumulate layers were formed through accumulation of 30–50% olivine, and it may be inferred that the differences in Gd/Yb ratios between these layers are the result of this process as proposed by Arndt and Lesher [26].

5.4. Liquidus temperatures of the komatiite melts and the plume model for their formation

Assuming that the Fe/Mg ratio in a primitive magma is directly related to its liquidus temperature [27] and using the technique proposed by Nisbet et al. [28] and Abbott et al. [29] we estimate average liquidus temperatures of the erupted komatiite liquids to be 1550 ± 20°C. This corresponds to a potential temperature of 1770 ± 20°C assuming that the liquidus temperature is directly related to potential temperature [25,29]. This implies in turn that the source of the Kostomuksha komatiites was substantially hotter than the ambient mantle (which had a potential temperature of 1540°C at 2.8 Ga, [30]). Such conditions, when ascending mantle material is > 200°C hotter than the surrounding mantle, are consistent with the plume model [31], which is now thought to be the essential mechanism of formation of large igneous provinces [8,32]. Thus we propose that a starting mantle plume was also responsible for the formation of the Kostomuksha plateau. The melting was initiated at a depth of 200–300 km. The universal Al–Sc–HREE depletion in the komatiites suggests that the magmas separated from the source still in the garnet stability field. Melting of the basalts probably proceeded all the way up to the surface. The close spatial and temporal association of komatiites and basalts could be accounted for by a model proposed by Campbell et al. [33]. Accordingly, a starting plume consists of a hot axial jet, capped by a large head into which cooler surrounding mantle is entrained. Komatiites form by melting in the high-temperature axis and basalts by melting in the cooler head. As the head is first to deliver the magmas to the surface, this model also explains the sequence and relative proportions of erupting magmas, in which basalts are volumetrically dominant and occupy the lowermost part of the belt. It should be noted, however, that the entrainment mechanism appears to be inconsistent with more recent fluid dynamic work [34].

5.5. Buoyancy of the Kostomuksha plateau

The buoyancy of the oceanic lithosphere is a function of its age and density distribution [35]. Newly formed, hot plates are initially buoyant. With time, the oceanic lithosphere cools and becomes more susceptible to subduction; after ~ 100 Ma the plates are potentially negatively buoyant [7]. Furthermore, the density distribution is controlled by the composition and thickness of crustal and mantle layers. These are in turn defined by the mantle temperature at the place where the crust formed, such that hotter mantle produces thicker oceanic crust and more depleted lithospheric mantle [25,36]. Mantle that has undergone a higher degree partial melting, has less residual garnet and less iron, and is less dense than more fertile mantle [35]. Therefore, it becomes more buoyant.

Because plumes are ~ 200–300°C hotter than the ambient mantle, they are able to produce much greater melt thickness than purely passive upwelling below mid-ocean ridges. Modern volcanic activity caused by ascending mantle plumes produces oceanic plateaux 15–40 km thick [37] compared with the thickness of ~ 7 km for the normal oceanic crust. Moreover, a hotter mantle in the Archaean [38] would have resulted in still higher degrees of partial melting and therefore a much larger volume of Archaean oceanic crust and a more depleted lithosphere beneath. Due to the presence of thick depleted lithospheric roots, some Archaean oceanic plateaux therefore might have been still too buoyant to subduct when they reached a convergent continental margin. In this case two scenarios are possible. They either clog the subduction zone and start subducting in the opposite direction as it happened to Ontong Java [39], or they dock with the continent and obduct onto it as is documented for the Caribbean and Wrangelia plateaux [40,41].

There is thus the interrelationship between the volume of mantle melting, thickness of oceanic crust and the lithospheric buoyancy. Cloos [42] and Abbott and Mooney [6] established that oceanic plates with crust over ~ 25 km thick are unsubductable regardless of their age. Employing the technique of Abbott

et al. [29] we estimate the crustal thickness for the Kostomuksha plateau. It varies from 54 km for the hottest core of the plume represented by the komatiites to 9 km as derived from the basalts, with an average value of ~30 km. Therefore, this postulated plateau meets the crustal thickness requirement to resist subduction and commence a long-term residence at the Earth's surface.

5.6. Source characteristics of the Kostomuksha lavas

The slightly elevated and nearly uniform initial ϵNd values of +2.8 to +3.4 in the komatiites and basalts imply that they originated from a well-mixed, long-term depleted mantle reservoir. Similar isotopic compositions have been found in other Archaean terranes, particularly the Abitibi (e.g., [43]) and Olondo [44] and uncontaminated parts of the Belingwe [45] and Kambalda [46] belts. Similarly uniform ϵNd(T) values have been found by Abouchami et al. for the 2.1 Ga old Birimian terrane of Western Africa [3]. Blichert-Toft and Albarède [47] have concluded on the basis of a statistical analysis of available Nd data that the Precambrian mantle was isotopically more homogeneous than present-day mantle because of more vigorous convective mixing.

Stein and Hofmann [5] have proposed that extensive, episodic new additions to the continental crust can be traced by a Nd-isotopic evolution line, which goes approximately through the initial ratios noted above and ends up near the locus of present-day ''prevalent mantle'' (PREMA) proposed by Wörner et al. [48]. Stein and Hofmann referred to these events as ''MOMO'' (major orogeny — mantle overturn), and it is convenient to display the isotopic compositions relative to this hypothetical MOMO evolution line, irrespective of its true meaning. Fig. 7 shows the isotopic compositions in this manner [ϵNd(CHUR) − ϵNd(MOMO)]. This illustrates the similarity of the juvenile Archaean greenstone belts and Phanerozoic oceanic plateaux, and the contrast to island arc, MORB, and those Precambrian greenstones, which are thought to be contaminated by pre-existing continental crust. The reason for the heterogeneity of the various young volcanic provinces is not the subject of this paper, but it is generally interpreted to be related to recycling of oceanic and continental crust and/or lithospheric material (see

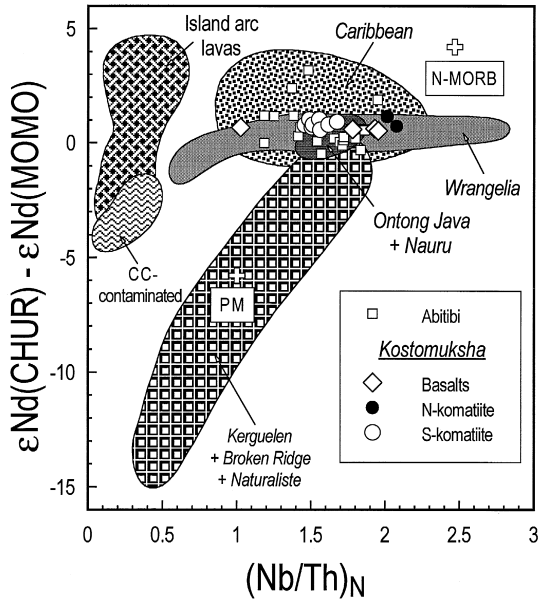

Fig. 7. $(Nb/Th)_N$ vs. ϵNd(CHUR) − ϵNd(MOMO) data. The parameters of the PREMA reservoir are adopted from Wörner et al. [48] to be the following: $^{143}Nd/^{144}Nd = 0.51294$; $^{147}Sm/^{144}Nd = 0.2066$. *CC* = average continental crust of Rudnick and Fountain [64]; primitive mantle (*PM*) and N-MORB estimates are from Hofmann [63]. The data sources used here and in Fig. 8 are available upon request or as an EPSL Online background data set (URL: http://www.elsevier.nl/locate/epsl, mirror site: http://www/elsevier.com/locate/epsl).

review in Ref. [49]). The reason for the comparative homogeneity of Pacific oceanic plateaux and juvenile Archaean greenstones has been suggested by Stein and Hofmann to be the mixing of plume material during ascent of the plume head from the deep mantle. If this is correct, then these greenstones are good representatives of the convecting part of the Archaean mantle.

The composition of this Archaean mantle can be further characterized by the Nb/La and Nb/Th ratios of the greenstones (Fig. 8)(The data sources used in Figs. 7 and 8 are available as **EPSL Online Background Dataset** [1].) Again, these are quite similar in the Kostomuksha plateau and in the Abitibi greenstones. The normalized Nb/La ratios are

[1] URL: http://www.elsevier.nl/locate/epsl, mirror site: http://www/elsevier.com/locate/epsl

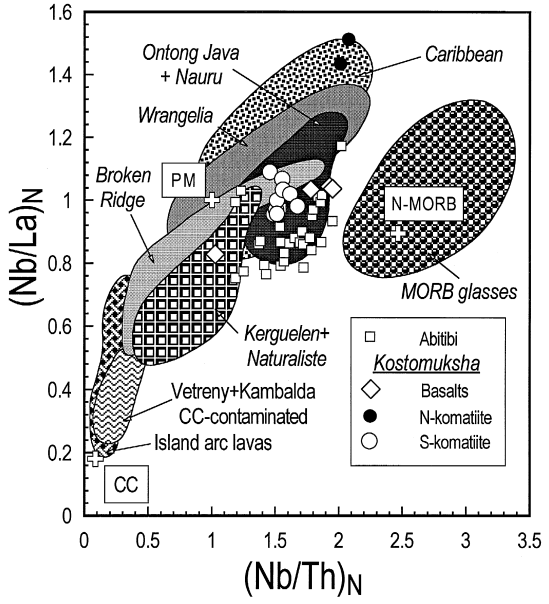

Fig. 8. $(Nb/Th)_N$ vs. $(La/Nb)_N$ data for Kostomuksha and Abitibi lavas compared with recent oceanic plateaux, MORB, island arc tholeiites and crustally contaminated lavas.

roughly equal to unity, but the Nb/Th ratios are significantly greater than unity, thus suggesting the presence of a relative Nb excess in the Archaean mantle. This suggestion is pursued further in the following section.

5.7. Lead isotopes and inferred Nb / U ratios

The Pb-isotope data plotted in Fig. 6 show that leachates nearly coincide with and extend the $^{207}Pb/^{204}Pb$ vs. $^{206}Pb/^{204}Pb$ isochron formed by the residues with an age of 2813 ± 78 Ma. This indicates that the U and/or Pb mobilization giving rise to the isotope separation of the leachates occurred shortly after the magmatic event and was probably contemporary with the metamorphic reworking dated at 2757 ± 113 Ma.

The initial Pb-isotope composition cannot be precisely determined from these data but can be estimated using simplified Pb evolution models. The simplest of these, the two-stage model, where the first stage extends from the meteorite age of 4.56 Ga to the emplacement age of 2.80 Ga [50], is inconsistent with conformable Pb evolution. The solution advocated by Stacey and Kramers [50] may be replaced by the assumption of a younger ''age of the Earth'' (actually, the age of core formation) advocated by some authors [51,52]. This view is consistent with the recognition that the Earth accretion and subsequent core formation probably lasted several tens of millions of years. We assume here an ''age of the mantle'' of 4.50 Ga. A two-stage model then yields a time-integrated $^{238}U/^{204}Pb$ of the source of the lavas (μ_1) of 8.77 ± 0.02 (4.50–2.80 Ga). This value implies a relatively unradiogenic Pb composition of the Kostomuksha source. It is somewhat higher than that in the Abitibi (8.59, [53]) and Olondo belts (8.60, [44]) and the Ontong Java and Manihiki plateaux (8.63, [54,55]), but is similar to that in uncontaminated Belingwe (8.74, [45]) and Kambalda (8.70, [56]) lavas, and in the Wrangelia and Caribbean (8.71, [41,57]) plateaux. We suggest therefore that the Kostomuksha plateau originated away from large continental terranes and no older felsic rocks were involved in the petrogenesis of these lavas.

Fig. 6 shows the corresponding ^{208}Pb data. In this diagram, the leachates and the komatiite residues appear to form linear correlations with slightly different slopes. $^{232}Th/^{238}U$ ratios calculated are 3.26 ± 0.26 for the leachates and 3.01 ± 0.19 for the residues. Although this difference is not statistically significant, we prefer to use the data for the residues to give the best estimate of the actual Th/U ratios of the rocks. We now calculate ''real'' U concentrations from the measured Th abundances and Pb isotope data (Table 1). For this we use the above assumption that the Pb isotopes of the komatiite residues represent the original unaltered rocks without serious bias, and the previously made inference based on Fig. 3 that Th has been immobile.

Using estimated U concentrations we calculate ''true'' Nb/U ratios in the rocks. The average values range from 43 for the basalts (excluding one aberrant sample 91145) and 47 for the Northern komatiites to 35 for the Southern komatiites (Table 1). Values similar to the lower end of this range are also found in basalts from the Ontong Java (Nb/U = 36), Caribbean (= 39) and Wrangelia (= 33) plateaux, whereas the higher Nb/U values in Kostomuksha are indistinguishable from recent MORB and OIB and from the uncontaminated part of the Kambalda sequence [58] with Nb/U of ~ 47.

Nb/U systematics in mafic–ultramafic lavas can be used to deduce the history of continental crustal growth [59]. This is attributed to the fact that Nb/U ratio has changed from the primitive value of ~30 prior to any continent formation to ~47 in the present-day mantle in response to the removal of the continental crust with Nb/U of ~10. However, it is unclear whether it has grown irreversibly over time [60] or was formed in the early Archaean and then was maintained in a steady state through continuous formation and recycling back into the mantle [61]. The high Nb/U ratios detected in lavas from the Kambalda [58] and Kostomuksha provinces provide some evidence in support of the latter model. However, we recognize that Nb/U data alone cannot unequivocally resolve this important controversy. The present-day mass of the high-Nb/U mantle reservoir is only loosely constrained to be between 30% and 70% of the total mantle [49]. If the mass of the complementary mantle reservoir increased proportionally with the mass of the continental crust, then Nb/U ratios of the mantle are relevant to the chemistry but not the growth rate of the continental crust. However, such a scenario may be difficult to reconcile with current ideas about mantle convection. In any case, if the mass of the residual, and presumably convecting mantle reservoir was constant through time, then the remarkable similarity of Nb/U ratios of Archaean and modern mantle-derived magmas strongly suggests a constant continental mass since the Archaean.

5.8. The pseudostratigraphy of recent oceanic plateaux and Archaean greenstone belts

Most complete information about the internal structure and fate of oceanic plateaux comes from studies of recent obducted oceanic plates such as the Caribbean plateau [8,40]. The results of these studies also bear on the understanding of the processes of Archaean tectonics. One of the typical observations for the Archaean greenstone belts, including the Kostomuksha belt, is the absence of ultramafic cumulates and tectonite peridotites [17], which constitute the lower part of ophiolite sequences. This fact suggests that Archaean greenstone belts are not fragments of *thin* oceanic crust analogous to what is found in ophiolites. Evidence from the Caribbean plateau suggests that, in contrast to suprasubduction zone ophiolites involving thin crust, in the case of thickened komatiite–basalt crust only the upper part is imbricated and obducted, whereas the deeper zones are subducted or tectonically underplated beneath active continental margins [40,62]. Kimura et al. [17] suggested that the décollement zone occurs at the base of the hydrothermal circulation cells, where rheologically weak altered volcanic rocks are underlain by fresh mafic–ultramafic cumulates. We argue that this was also the case for the Kostomuksha plateau, and the documented shear zone represents the detachment surface at the boundary between the upper and lower crustal parts of this fossil plateau.

Most Phanerozoic ophiolites, which are commonly recognized as remnants of oceanic crust, contain sheeted dike complexes emplaced during crust formation at spreading ridges. These dikes are virtually absent from both modern oceanic plateaux and Archaean greenstone belts. Instead, these contain huge amounts of horizontal lava flows and related hypabyssal and abyssal sills. This observation suggests that the magma supply was enormous and greatly exceeded the extension rate necessary to accommodate it [8]. Archaean greenstone belts probably have little in common with Phanerozoic ophiolites. In contrast, they share many geological and geochemical characteristics with a different type of oceanic crust, such as is represented by oceanic plateaux.

6. Conclusions

(1) The Kostomuksha greenstone belt represents an ancient accretionary complex, which reveals coexistence of allochthonous oceanic material with terrigenous sedimentary deposits.

(2) The erupted komatiite magma contained ~27% MgO, had a liquidus temperature of ~1550°C and was formed in a hot axial part of a deep mantle plume in equilibrium with residual garnet. This plume had the thermal potential to produce oceanic crust with an average thickness of ~30 km and permanently buoyant refractory lithospheric mantle roots.

(3) The komatiites and basalts have isotope and chemical signatures resembling those of Pacific oceanic plateaux lavas; no crustal rocks were involved in their petrogenesis.

(4) The magma source regions of the Kostomuksha lavas have experienced a degree of depletion due to continental crust formation comparable with those found in the modern mantle as evidenced by Nb–Th–U–Pb relationships. These and data on the Kambalda province suggest that a volume of continental crust similar to the present-day value already existed by the end of the Archaean.

(5) We propose that the Kontokky terrane represents a remnant of an uppermost crustal part of an Archaean oceanic plateau. It was delaminated from its lower part and accreted to and obducted onto an ancient continental convergent margin represented by the Gimola terrane. The felsic rocks within the Kontokky terrane represent collision-related volcanism that erupted through the accreted plateau material and was caused by partial melting of the continental crustal rocks during obduction and imbrication of the upper part and underplating of the lower part of the plateau.

Acknowledgements

Thanks are due to V. Furman for help during the field work and for supply of the drill core samples. Thorough and constructive reviews by John Ludden, Dallas Abbott and Claude Herzberg resulted in substantial improvements of the original version of the manuscript. This study was supported by Alexander-von-Humboldt and Max-Planck-Institut für Chemie fellowships to ISP and by the Russian Foundation for Fundamental Research. *[FA]*

References

[1] S.R. Taylor, S.M. McLennan, The Continental Crust: Its Composition and Evolution, Blackwell, Boston, MA, 1985, 312 pp.
[2] Z. Ben-Avraham, A. Nur, D. Jones, A. Cox, Continental accretion: From oceanic plateaus to allochthonous terranes, Science 213 (1981) 47–54.
[3] W. Abouchami, M. Boher, A. Michard, F. Albarède, A major 2.1 Ga event of mafic magmatism in West Africa: An early stage of crustal accretion, J. Geophys. Res. 95 (1990) 17605–17629.
[4] M. Boher, W. Abouchami, A. Michard, F. Albarède, N.T. Arndt, Crustal growth in West Africa at 2.1 Ga, J. Geophys. Res. 97 (1992) 345–369.
[5] M. Stein, A.W. Hofmann, Mantle plumes and episodic crustal growth, Nature (London) 372 (1994) 63–68.
[6] D.H. Abbott, W. Mooney, The structural and geochemical evolution of the continental crust: Support for the oceanic plateau model of continental growth, Rev. Geophys. 33 (1995) 231–242.
[7] Abbott, R. Drury, W.D. Mooney, Continents as lithological icebergs: The importance of buoyant lithospheric roots, Earth Planet. Sci. Lett. 149 (1997) 15–27.
[8] A.D. Saunders, J. Tarney, A.C. Kerr, R.W. Kent, The formation and fate of large oceanic igneous provinces, Lithos 37 (1996) 81–95.
[9] G. Schubert, D. Sandwell, Crustal volumes of the continents and of oceanic and continental submarine plateaus, Earth Planet. Sci. Lett. 92 (1989) 234–246.
[10] M.F. Coffin, O. Eldholm, Scratching the surface: Estimating dimensions of large igneous provinces, Geology 21 (1993) 515–518.
[11] Y. Lahaye, N.T. Arndt, G. Byerly, C. Chauvel, S. Fourcade, G. Gruau, The influence of alteration on the trace-element and Nd-isotopic compositions of komatiites, Chem. Geol. 126 (1995) 43–64.
[12] Y. Lahaye, N.T. Arndt, Alteration of a komatiite flow from Alexo, Ontario, J. Petrol. 37 (1996) 1261–1284.
[13] R. Gorbatschev, S. Bogdanova, Frontiers in the Baltic Shield, Precambrian Res. 64 (1993) 3–21.
[14] V.Y. Gor'kovets, M.B. Raevskaya, The Gimola–Kostomuksha greenstone belt, in: V.A. Sokolov (Ed.), Volcanism of Archean Greenstone Belts in Karelia, Nauka, Leningrad, 1981, pp. 68–74.
[15] I.S. Puchtel, A.A. Shchipansky, A.V. Samsonov, D.Z. Zhuravlev, The Karelian granite–greenstone terrain in Russia, in: M.J. deWit, L.D. Ashwal (Eds.), Greenstone Belts, Clarendon, Oxford, 1997, pp. 699–706.
[16] A.V. Samsonov, E.V. Bibikova, I.S. Puchtel, A.A. Shchipansky, D.Z. Zhuravlev, V.N. Furman, Petrology and geochronology of felsic magmatic rocks from the Kostomuksha greenstone belt, western Karelia, Petrology (1997, submitted).
[17] G. Kimura, J.N. Ludden, J.-P. Desroshers, R. Hori, A model of ocean-crust accretion for the Superior province, Canada, Lithos 30 (1990) 337–355.
[18] K.P. Jochum, H.-J. Laue, H.M. Seufert, A.W. Hofmann, First analytical results using a multi-ion counting system of a spark source mass spectrometer, Fresenius J. Anal. Chem. 350 (1994) 642–644.
[19] I.S. Puchtel, K.M. Haase, A.W. Hofmann, C. Chauvel, V.S. Kulikov, C.-D. Garbe-Schönberg, A.A. Nemchin, Petrology and geochemistry of crustally contaminated komatiitic basalts from the Vetreny Belt, southeastern Baltic Shield: Evidence for an early Proterozoic mantle plume beneath rifted Archean continental lithosphere, Geochim. Cosmochim. Acta 61 (1997) 1205–1222.
[20] I.S. Puchtel, N.T. Arndt, A.W. Hofmann, K.M. Haase, A. Kröner, V.S. Kulikov, V.V. Kulikova, C.-D. Garbe-Schönberg, A.A. Nemchin, Petrology of mafic lavas within the Onega plateau, central Karelia: Evidence for the 2.0 Ga

plume-related continental crustal growth in the Baltic Shield, Contrib. Mineral. Petrol. (1997, in press).
[21] N.T. Arndt, Differentiation of komatiite flows, J. Petrol. 27 (1986) 279–301.
[22] P. Beattie, C. Ford, D. Russell, Partition coefficients for olivine–melt and orthopyroxene–melt systems, Contrib. Mineral. Petrol. 109 (1991) 212–224.
[23] D.H. Green, Genesis of Archean peridotitic magmas and constraints on Archean geothermal gradients and tectonics, Geology 3 (1975) 15–18.
[24] C. Herzberg, Generation of plume magmas through time: an experimental perspective, Chem. Geol. 126 (1995) 1–16.
[25] D. McKenzie, M.J. Bickle, The volume and composition of melt generated by extension of the lithosphere, J. Petrol. 29 (1988) 625–679.
[26] N.T. Arndt, C.M. Lesher, Fractionation of REE's by olivine and the origin of Kambalda komatiites, Western Australia, Geochim. Cosmochim. Acta 56 (1992) 4191–4204.
[27] P.L. Roeder, R.F. Emslie, Olivine–liquid equilibrium, Contrib. Mineral. Petrol. 29 (1970) 275–282.
[28] E.G. Nisbet, M.J. Cheadle, N.T. Arndt, M.J. Bickle, Constraining the potential temperature of the Archaean mantle: A review of the evidence from komatiites, Lithos 30 (1993) 291–307.
[29] D.H. Abbott, L. Burgess, J. Longhi, W.H.F. Smith, An empirical thermal history of the Earth's upper mantle, J. Geophys. Res. 99 (1994) 13835–13850.
[30] F.M. Richter, A major change in the thermal state of the Earth at the Archean–Proterozoic boundary: Consequences for the nature and preservation of continental lithosphere, J. Petrol., Spec. Lithosphere Iss. (1988) 39–52.
[31] I.H. Campbell, R.W. Griffiths, Implications of mantle plume structure for the evolution of flood basalts, Earth Planet. Sci. Lett. 99 (1990) 79–93.
[32] M.F. Coffin, O. Eldholm, Large igneous provinces: crustal structure, dimensions and external consequences, Rev. Geophys. 32 (1994) 1–36.
[33] I.H. Campbell, R.W. Griffiths, R.I. Hill, Melting in an Archaean mantle plume: head it's basalts, tails it's komatiites, Nature (London) 339 (1989) 697–699.
[34] C.G. Farnetani, M.A. Richards, Thermal entrainment and melting in mantle plumes, Earth Planet. Sci. Lett. 136 (1995) 251–267.
[35] E.R. Oxburgh, E.M. Parmentier, Compositional density stratification in oceanic lithosphere — causes and consequences, J. Geol. Soc. London 133 (1977) 343–355.
[36] C.H. Langmuir, E.M. Klein, T. Plank, Petrological constraints on mid-ocean ridge basalts: constraints on melt generation beneath ocean ridges, in: Mantle Flow and Melt Generation at Mid-Ocean Ridges, Geophys. Monogr. (1992) 183–280.
[37] R.S. White, D. McKenzie, R.K. O'Nions, Ocean crust thickness from seismic measurements and rare earth element inversions, J. Geophys. Res. 97 (1992) 19683–19715.
[38] M.J. Bickle, Implications of melting for stabilisation of lithosphere and heat loss in the Archaean, Earth Planet. Sci. Lett. 80 (1986) 314–324.
[39] C.R. Neal, J.J. Mahoney, L.W. Kroenke, R.A. Duncan, M.G. Petterson, The Ontong Java Plateau, in: J.J. Mahoney, M. Coffin (Eds.), Am. Geophys. Union Monogr. on Large Igneous Provinces (1997, in press).
[40] A.C. Kerr, J. Tarney, G.F. Marriner, A. Nivia, A.D. Saunders, The Caribbean–Colombian Cretaceous igneous province: The internal anatomy of an oceanic plateau, in: J.J. Mahoney, M. Coffin (Eds.), Am. Geophys. Union Monogr. on Large Igneous Provinces (1997, in press).
[41] J.C. Lassiter, D.J. DePaolo, J.J. Mahoney, Geochemistry of the Wrangelia flood basalt province: Implications for the role of continental and oceanic lithosphere in flood basalt genesis, J. Petrol. 36 (1995) 983–1009.
[42] M. Cloos, Lithospheric buoyancy and collisional orogenesis: Subduction of oceanic plateaus, continental margins, island arcs, spreading ridges, and seamounts, Geol. Soc. Am. Bull. 105 (1993) 715–737.
[43] J.D. Vervoort, W.M. White, R.I. Thorpe, Nd and Pb isotope ratios in the Abitibi greenstone belt: new evidence for very early differentiation of the Earth, Earth Planet. Sci. Lett. 128 (1994) 215–229.
[44] I.S. Puchtel, D.Z. Zhuravlev, Petrology of mafic–ultramafic metavolcanics and related rocks from the Olondo greenstone belt, Aldan Shield, Petrology 1 (1993) 308–348.
[45] C. Chauvel, B. Dupré, N.T. Arndt, Pb and Nd isotopic correlation in Belingwe komatiites and basalts, in: M.J. Bickle, E.G. Nisbet (Eds.), The Geology of the Belingwe Greenstone Belt, Zimbabwe — A Study of the Evolution of Archaean Continental Crust, A.A. Balkema, Rotterdam, 1993, pp. 167–174.
[46] C.M. Lesher, N.T. Arndt, REE and Nd isotope geochemistry, petrogenesis and volcanic evolution of contaminated komatiites at Kambalda, Western Australia, Lithos 34 (1995) 127–158.
[47] J. Blichert-Toft, F. Albarède, Short-lived chemical heterogeneities in the Archean mantle with implications for mantle convection, Science 263 (1994) 1593–1596.
[48] G. Wörner, A. Zindler, H. Staudigel, H.-U. Schmincke, Sr, Nd, and Pb isotope geochemistry of Tertiary and Quaternary alkaline volcanics from West Germany, Earth Planet. Sci. Lett. 79 (1986) 107–119.
[49] A.W. Hofmann, Mantle geochemistry: the message from oceanic volcanism, Nature (London) 385 (1997) 219–229.
[50] J.S. Stacey, J.D. Kramers, Approximation of terrestrial lead isotope evolution by a two-stage model, Earth Planet. Sci. Lett. 26 (1975) 207–221.
[51] C.J. Allègre, G. Manhès, C. Göpel, The age of the Earth, Geochim. Cosmochim. Acta 59 (1995) 1445–1456.
[52] S.J.G. Galer, S.L. Goldstein, Influence of accretion on lead in the Earth, Geophys. Monogr. 95 (1996) 75–98.
[53] J. Carignan, N. Machado, C. Gariépy, U–Pb isotopic geochemistry of komatiites and pyroxenes from the southern Abitibi greenstone belt, Canada, Chem. Geol. 126 (1995) 17–27.
[54] J.J. Mahoney, K.J. Spenser, Isotopic evidence for the origin of the Manihiki and Ontong Java oceanic plateaus, Earth Planet. Sci. Lett. 104 (1991) 196–210.

[55] J.J. Mahoney, M. Storey, R.A. Duncan, K.J. Spencer, M. Pringle, Geochemistry and age of the Ontong Java Plateau, in: The Mesozoic Pacific: Geology, Tectonics and Volcanism, Geophys. Monogr. 77 (1993) 233–261.
[56] N.J. McNaughton, K.M. Frost, D.I. Groves, Ground melting and ocellar komatiites: A lead isotopic study at Kambalda, Western Australia, Geol. Mag. 125 (1988) 285–295.
[57] B. Dupré, L.M. Echeverria, Pb isotopes of Gorgona island (Colombia): isotopic variations correlated with magma type, Earth Planet. Sci. Lett. 67 (1984) 186–190.
[58] P.J. Sylvester, I.H. Campbell, D.A. Bowyer, Niobium/uranium evidence for early formation of the continental crust, Science 275 (1997) 521–523.
[59] A.W. Hofmann, K.-P. Jochum, M. Seufert, W.M. White, Nb and Pb in oceanic basalts: New constraints on mantle evolution, Earth Planet. Sci. Lett. 79 (1986) 33–45.
[60] S. Moorbath, Ages, isotopes and evolution of Precambrian continental crust, Chem. Geol. 20 (1977) 151–187.
[61] R.L. Armstrong, Radiogenic isotopes: the case for crustal recycling on a near-steady-state no-continental-growth, Philos. Trans. R. Soc. London, Ser. A 301 (1981) 443–472.
[62] K. Burke, Tectonic evolution of the Caribbean, Annu. Rev. Earth Planet. Sci. 16 (1988) 201–230.
[63] A.W. Hofmann, Chemical differentiation of the Earth: The relationship between mantle, continental crust and oceanic crust, Earth Planet. Sci. Lett. 90 (1988) 297–314.
[64] R.L. Rudnick, D.M. Fountain, Nature and composition of the continental crust: a lower crustal perspective, Rev. Geophys. 33 (1995) 267–309.